Immediate stress dissipation in dual cross-link hydrogels controls osteogenic commitment of mesenchymal stem cells

Chiara Pizzolitto [a], Francesca Scognamiglio [a], Pasquale Sacco [a,b,c,*], Sara Lipari [b,1], Maurizio Romano [b], Ivan Donati [b], Eleonora Marsich [a]

[a] Department of Medicine, Surgery and Health Sciences, University of Trieste, Piazza dell'Ospitale 1, I-34129 Trieste, Italy
[b] Department of Life Sciences, University of Trieste, Via Licio Giorgieri 5, I-34127 Trieste, Italy
[c] AREA Science Park, loc. Padriciano 99, I-34149 Trieste, Italy

ARTICLE INFO

Keywords:
Hydrogel
Temporary/permanent cross-linkers
Material viscoplasticity
Mesenchymal stem cells
Osteogenic differentiation
Mechanotransduction

ABSTRACT

In vitro studies of mesenchymal stem cells (MSCs) differentiation have been predominantly performed with non-physiologically elastic materials. Here we report the effect of different viscoplastic ECM mimics on the osteogenic engagement of MSCs in 2D. We have developed soft hydrogels, composed of a lactose-modified chitosan, using a combination of permanent and temporary cross-links. The presence of temporary cross-links has a minor effect on the shear modulus of the hydrogels, but causes an immediate relaxation (dissipation) of the applied stress. This material property leads to early osteogenic commitment of MSCs, as evidenced by gene expression of runt-related transcription factor 2 (RUNX2), type 1 collagen (COL1A1), osteocalcin (OCN), alkaline phosphatase enzyme activity (ALP) and calcium deposit formation. In contrast, cells cultured on purely elastic hydrogels with only permanent cross-link begin to differentiate only after a longer period of time, indicating a dissipation-mediated mechano-sensing in the osteogenic commitment of MSCs.

1. Introduction

Mechanical signals from the extracellular matrix (ECM) surrounding cells are crucial for their behaviour, by influencing biology, stemness, tissue development and regeneration or by triggering the onset of various diseases (Brusatin, Panciera, Gandin, Citron, & Piccolo, 2018; Discher, Janmey, & Wang, 2005; Discher, Mooney, & Zandstra, 2009; Dupont et al., 2011; Engler, Sen, Sweeney, & Discher, 2006; Mammoto & Ingber, 2010; Panciera, Azzolin, Cordenonsi, & Piccolo, 2017; Swift et al., 2013). Biologically, cells interact with ECMs by pulling through the actomyosin-based contractility *via* integrin-based adhesions, and by pushing through actin and microtubules polymerization (Chaudhuri, Cooper-White, Janmey, Mooney, & Shenoy, 2020). On the matrix side, living tissues behave like viscoelastic materials exhibiting a time- and frequency-dependent response to deformation, dissipating the forces exerted by cells. Although viscoelasticity has been found to be a nearly universal property of living tissues, most of our understanding of cell biology comes from unnatural, purely elastic materials.

The response of cells to the viscous and dissipative properties of the ECM is an attractive topic nowadays (Cantini, Donnelly, Dalby, & Salmeron-Sanchez, 2020). In this scenario, 2D polyacrylamide hydrogels with constant elastic but varying loss modulus were used to study cell morphology, proliferation, differentiation potential and migration (Cameron, Frith, & Cooper-White, 2011; Cameron, Frith, Gomez, Yap, & Cooper-White, 2014). The entrapment of linear polymer chains in polyacrylamide gels (semi-interpenetrating networks) was used as an alternative mechanism to regulate viscous dissipation, affecting cell phenotype and mechanosensing (Charrier, Pogoda, Wells, & Janmey, 2018). Similarly, alginate hydrogels with adjustable stress relaxation due to physical cross-linking and different nanoscale architecture have been developed and used as 2D and 3D networks to study cell spreading, proliferation, yes-associated protein (YAP) nuclear translocation, osteogenic differentiation of mesenchymal stem cells (MSCs) and cartilage matrix formation by chondrocytes (Bauer et al., 2017; Chaudhuri et al., 2015, 2016; Lee, Gu, Mooney, Levenston, & Chaudhuri, 2017). Recently, chitosan-based viscoelastic hydrogels with different chemical

* Corresponding author at: Department of Life Sciences, University of Trieste, Via Licio Giorgieri 5, I-34127 Trieste, Italy.
E-mail address: psacco@units.it (P. Sacco).
[1] Present address: Pole of Pharmacology and Therapeutics, Institut de Recherche Expérimentale et Clinique (IREC), Université Catholique de Louvain (UCLouvain), B-1200 Brussels, Belgium.

Accepted 16 November 2022

compositions and adjustable dissipation energy have been used to study cell spreading, YAP translocation and focal adhesion assembly (Sacco, Baj, et al., 2020). In addition, poly(ethylene glycol)-based hydrogels with viscoelasticity provided by adaptive boronate ester crosslinking or photoinduced addition-fragmentation chain transfer reaction have been used to study cell adhesion, morphology, and mechanosensing (Marozas, Anseth, et al., 2019; Marozas, Cooper-White, et al., 2019).

Materials that exhibit plastic (permanent) deformation when the applied stress is removed are a subset of viscoelastic materials. Mechanistically, networks consisting of only weak cross-links can be considered to be viscoplastic, while single or dual networks consisting of a combination of covalent and weak cross-links may or may not be viscoplastic, depending on the molecular architecture (Chaudhuri et al., 2020). In recent years, viscoplasticity has been found to be important in the interaction between cells and ECM. Indeed, cells have been found to foster plastic remodeling of the ECM, by inducing the realignment of matrix fibers in collagen and fibrin gels (Mohammadi, Arora, Simmons, Janmey, & McCulloch, 2015; Notbohm, Lesman, Tirrell, & Ravichandran, 2015; Petroll, Cavanagh, & Jester, 2004), through force transmission *via* the actin/β1-integrin axis, without entailing proteolysis by matrix metalloproteinases (Nam, Lee, Brownfield, & Chaudhuri, 2016). Furthermore, recent evidence has shown that viscoplasticity plays a pivotal role in regulating MSCs spreading and the related expression of many genes, cancer cells invasion in 3D confining microenvironments in a protease-independent manner and fibroblast activation in fibrosis (Grolman, Weinand, & Mooney, 2020; Jia et al., 2021; Wisdom et al., 2018). Although the viscoplasticity of ECM is recognized as an important mechano-controller in guiding cell fate decisions, it is often underestimated compared to simple viscoelasticity, so basic knowledge needs to be built to extend the current state of the art.

Here we report a novel viscoplastic, double cross-linked hydrogel system with adjustable degree of immediate stress dissipation and investigate the effects of viscoplasticity on osteogenic commitment of MSCs in 2D culture conditions. The hydrogel consists of a lactose-modified chitosan (CTL) (Furlani, Sacco, Cok, et al., 2019; Furlani, Sacco, Scognamiglio, et al., 2019; Pizzolitto et al., 2020; Sacco, Cok, et al., 2020; Sacco, Furlani, Paoletti, & Donati, 2019) with a combination of genipin (permanent) and boric acid (temporary) cross-links (Sacco, Furlani, et al., 2020). While permanent junctions essentially contribute to the elastic response of the hydrogels under loading, the rapid binding/unbinding dynamics of temporary cross-links allow to finely tune the immediate matrix flow with significant relaxation (dissipation) of stress. We show that this material trait is a crucial feature that temporally guides stem cells in the commitment toward an osteogenic phenotype. We provide evidence that the rapid relaxation of stress, which depends on the amount of temporary cross-links, in this hydrogel system affects important aspects of MSC biology, such as gene expression, enzyme production, mineralized matrix deposition and cell morphology.

2. Materials and methods

2.1. Materials

Hydrochloride form of lactose-modified chitosan, CTL (CAS Registry Number 2173421.37-7) was kindly provided by BiopoLife s.r.l. (Trieste, Italy). The chemical composition of CTL was determined by ^{1}H NMR spectroscopy and resulted: fraction of deacetylated units (F_D) 0.21, fraction of lactose-modified units (F_L) 0.63 and fraction of acetylated units (F_A) 0.16. The calculated molar mass of CTL repeating unit ($MW_{r.u.}$) resulted 403 g/mol. The physical properties of CTL were determined by viscometry: the intrinsic viscosity, [η], of CTL was measured at T = 25 °C by means of a CT 1150 Schott Geräte automatic measuring apparatus and a Schott capillary viscometer (Furlani, Sacco, Cok, et al., 2019) and resulted 344 mL/g. The molar mass of CTL was estimated to be at around 800,000 g/mol (Sacco, Furlani, et al., 2020). Genipin (purity 98%) was from Challenge Bioproducts Co., Ltd. (Taiwan). Boric acid, phosphate buffered saline (PBS), mannitol, sodium hydroxide, sodium chloride, magnesium chloride, Triton X-100, Tris buffer, dexamethasone, bovine serum albumin (BSA), poly-L-lysine solution, silver nitrate, sodium thiosulfate, Tween-20, Fast Blue BB Salt Hemi (ZnCl) salt, Naphtol AS-X phosphate, Oil Red O, hematoxylin, fibronectin from bovine plasma, AlamarBlue reagent, *p*-nitrophenylphosphate, formaldehyde, Normal Goat Serum, Bradford reagent and TRI Reagent were all purchased from Sigma-Aldrich (USA). Mesenchymal stem cell growth medium 2 was from PromoCell. DMEM (Dulbecco's Modified Eagle's Medium), Fetal Bovine Serum (FBS), streptomycin, penicillin and trypsin were from EuroClone (Italy). L-Ascorbic acid and β-glycerophosphate were form Fluka Biochemika. Hydrochloric acid and Propan-2-ol were from Carlo Erba (Italy).

2.2. Preparation of dual cross-link hydrogels

CTL solutions were prepared in 1× PBS buffer, pH 7.4 (Furlani, Sacco, Cok, et al., 2019). Briefly, CTL (150 mg) was solubilized in 3.5 mL of deionized water, the pH was then adjusted to 7.4 by adding aliquots of NaOH (1 or 5 M). Finally, 400 μL of 10× PBS and deionized water were added to have a final volume of 4 mL. The mixture composed of boric acid (80 mM) and mannitol (160 mM) was prepared in 1× PBS buffer, pH 7.4. Genipin (15.6 mM) was solubilized in 1× PBS. CTL and boric acid/mannitol/genipin (gelling mixture) was mixed through a Luer-Lock syringe system (Supplementary material, Appendix 1, for further details). In all tests, the final experimental conditions were: [genipin] = 1.56 mM, [CTL] = 3% w/v, [boric acid] = 0–8 mM, [mannitol] = 0–16 mM, respectively. The composition of the three gels is reported in Table S1 of the Supplementary material section.

2.3. Mechanical characterization

After mixing, the solutions were poured into 6-well plates and incubated for 24 h at T = 37 °C to allow gelation. The hydrogels were then cut by means of a disposable 20 mm diameter punch. The height of each cylinder resulted ~2.5 mm. All rheological tests were performed on an HAAKE MARS III rheometer (ThermoScientific) using a shagreened plate-plate apparatus ("HPP20 *profiliert*": diameter = 20 mm), at a reference temperature of 37 °C. To improve thermal control and avoid water evaporation from the gel, measurements were performed in a water-saturated environment formed by using a solvent trap containing a wet cloth. The gap between plates was adjusted by executing a series of short stress sweep test (frequency, ν = 1 Hz; stress, τ, range 1–5 Pa) to maximize the elastic response. For each sample, creep-compliance (τ = 100 Pa applied for 600 s followed by τ = 0 Pa for 600 s) and stress-relaxation (γ = 1% applied for 600 s) tests were performed. The mechanical spectra (frequency sweep test: τ = 4 Pa; ν = 0.01–100 Hz) were also recorded by measuring the dependence of the elastic (G′) and viscous (G″) response. The extension of the linear viscoelastic regime was determined by stress sweep tests carried out using a constant frequency of 1 Hz in the stress range 0.1–1000 Pa.

The Young's modulus of hydrogels was measured by performing compression tests using a Universal Testing Machine (Multitest 2.5-i) coupled with a 100 N load cell. The compression speed was set on 5 mm/min. The Young's modulus was calculated by measuring the slop of the stress-strain curve in the range 1–5% of strain.

2.4. Swelling experiments

The structural stability of hydrogels was verified in cell culture media (high glucose Dulbecco's Modified Eagle Medium, DMEM) at 37 °C for 21 days. After gelation, small cylinders from original samples were punched out (diameter = 10 mm, thickness ~ 2.5 mm), weighted (time zero) and immersed in DMEM (hydrogel/DMEM 1:4 v/v). At selected time points, the samples were removed from the incubation

medium, blotted to remove the excess of medium using a filter paper and weighed. The % swelling was calculated as the water uptake with respect to the initial weight in agreement with the formula

$$\text{Water uptake } (\%) = \frac{W_t - W_0}{W_0} \times 100$$

where W_t is the weight of samples at different time intervals and W_0 the dry weight of hydrogels at $t = 0$. All measurements were performed at least with $n = 10$.

2.5. Cell culture

Human mesenchymal stem cells from adipose tissue (hMSC-AT, PromoCell) were used as cell model for the *in vitro* experiments. Cells were cultured in mesenchymal stem cell growth medium supplemented with 1% penicillin/streptomycin, in a humidified atmosphere of 5% CO_2 at $T = 37$ °C. Cells between passages 2 and 4 were used in all experiments.

2.6. Plating of cells on 2D hydrogels

Hydrogels with different composition were assembled in sterile conditions and further sterilized under UV for 20 min after gelling. Hydrogels were next coated overnight at $T = 37$ °C with a 20 μg/mL fibronectin solution in PBS. Cells were retrieved from subconfluent culture by trypsinization (trypsine/EDTA 1× in PBS solution), counted and plated to a density of 7000 cells/cm^2 for viability tests and 15,000 cells/cm^2 for differentiation studies. After 24 h, the culture medium was replaced by an osteogenic medium to induce hMSC-AT differentiation, composed of DMEM high glucose supplemented with 50 μg/mL L-ascorbic acid, 10 mM β-glycerophosphate and 0.1 μM dexamethasone (Chaudhuri et al., 2016). The medium was changed every 3 days.

2.7. Evaluation of stem cells osteogenic differentiation

2.7.1. ALP test

The intracellular ALP activity of hMSCs-AT was measured using the protocol reported elsewhere (Porrelli, Gruppuso, Vecchies, Marsich, & Turco, 2021). Additional details in the Appendix 1 of Supplementary material.

2.7.2. Fast Blue and Von Kossa staining

Cells were probed for alkaline phosphatase by Fast Blue staining after 14 days of culture. Cells were detached from hydrogels by trypsinization and seeded atop poly-lysine-coated coverslips. Cells were next equilibrated in alkaline buffer (100 mM Tris-HCl, 100 mM NaCl, 0.1% Tween-20, 50 mM $MgCl_2$, pH 8.2) for 15 min and stained in 500 μg/mL napthol AS-MX phosphate and 500 μg/mL Fast Blue BB Salt Hemi (ZnCl) salt in alkaline buffer for 60 min. Cells were then washed in alkaline buffer and in PBS. Finally, cells were stained with hematoxylin for 2 min and washed in deionized water. Data are expressed as the percentage of ALP-positive cells to total cells. Images were acquired through a Zeiss Axiophot microscope (Carl Zeiss, Germany) using a 20× as objective.

Calcium deposits were detected by means of Von Kossa staining performed on cells atop hydrogels. After 14 days of incubation in osteogenic medium, cells were fixed with formaldehyde 4% v/v in PBS for 10 min and then equilibrated in distilled water. Finally, hydrogels were incubated with 1% silver nitrate solution and UV light-irradiated for 40 min. Cells were next washed with distilled water and 5% sodium thiosulphate solution added for 5 min. At the end of staining, hydrogels were washed with distilled water. Images were acquired through an Exacta Optech microscope equipped with a Pentax digital camera using a 4× as objective.

2.7.3. Gene expression analysis

A detailed description of gene expression analysis is reported in the Appendix 2 of Supplementary material.

2.8. Morphological analysis

Cells were seeded at a density of 7000 cells/cm^2 on hydrogels with different composition and cultured for 14 days. Cells were fixed at days 5 and 14 by formaldehyde 4% v/v in PBS for 10 min at room temperature. Then, hydrogels were washed 3× with PBS and permeabilized by Triton X-100 0.2% v/v in PBS for 15 min at room temperature. Next, hydrogels were washed with PBS and incubated with BSA 4% w/v + Normal Goat Serum 5% v/v in PBS (blocking solution) for 1 h at $T = 37$ °C. The blocking solution was then removed, and the samples washed with PBS. For the visualization of nuclei, cells were counterstained with Hoechst (33258) 1:100 in PBS. Finally, hydrogels were washed twice and stored in PBS. Images were acquired using a Nikon Eclipse Ti-E epifluorescence Live-imaging microscope using a 20× as objective. The area and diameter of the cells were calculated from the acquired images using Fiji-ImageJ software.

2.9. Proliferation assay

A detailed description of proliferation assay is reported in the Appendix 1 of Supplementary material.

2.10. Oil Red O staining

Cells were probed for neutral lipids by Oil Red O staining after 14 days of culture. Cells were detached from hydrogels by trypsinization and seeded atop poly-lysine-coated coverslips. Cells were next equilibrated in 60% isopropanol and stained in 1.8 mg/mL Oil Red O in 60% isopropanol for 30 min. Cells were then washed quickly in isopropanol 60% and in deionized water. Finally, cells were stained with hematoxylin for 2 min and washed in deionized water. Images were acquired through a Zeiss Axiophot microscope (Carl Zeiss, Germany) using a 20× as objective.

2.11. Statistical analysis

Statistical analysis and graph elaboration were performed using GraphPad Prism 9 (GraphPad Software, San Diego, CA). One-way ANOVA (analysis of variance) followed by Dunnett's or Tukey's multiple comparison *post hoc* tests were performed to evaluate differences among groups and the control. An unpaired Mann-Whitney two-tailed *t*-test was also performed to evaluate significant differences between two groups. Differences were considered significant for p values < 0.05.

3. Results and discussion

3.1. Temporary/permanent dual cross-linked hydrogels

The first aim of this study was to prepare hydrogel substrates suitable for 2D cell culture and to investigate the effects of mechanical characteristics on cell behaviour. To achieve this goal, a temporary/permanent dual cross-linked hydrogel system consisting of a lactose-modified chitosan (CTL) was used (Sacco, Furlani, et al., 2020). Mixtures of boric acid (*i.e.* the temporary linker) and genipin (*i.e.* the permanent linker) were prepared and rapidly mixed with CTL. Due to the different binding kinetics of the two cross-linkers, a two-step gelation occurs: (*i*) an immediate increase in viscosity due to the rapid binding of boric acid to the diols on the lateral (grafted) lactitol units of CTL (Furlani, Sacco, Cok, et al., 2019); and (*ii*) a slow strengthening of the network due to the temperature-assisted binding of genipin to the residual primary amino groups of CTL at neutral pH (Pizzolitto et al., 2020). The presence of mannitol in the mixture allows the formation of an immediate

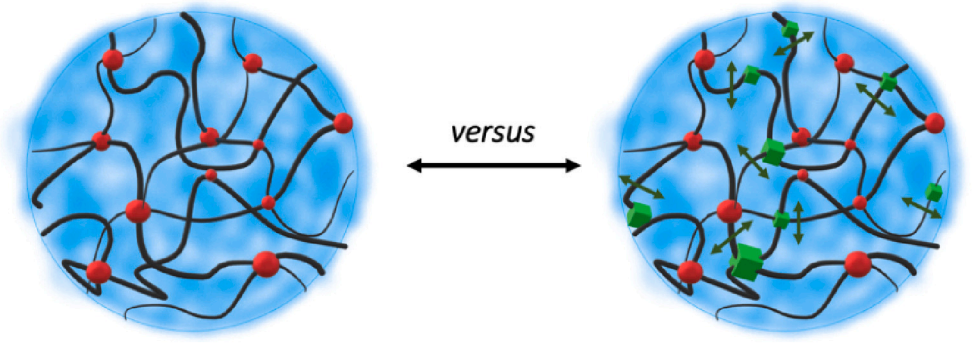

Scheme 1. Sketchy representation of the hypothetical internal network of the hydrogel systems investigated in this study. In the case of exclusively permanent, genipin-based, cross-links (red dots), the network is expected to behave like an elastic material under load with negligible relaxation of the applied stress. After the introduction of temporary boric acid cross-links (green cubes), which are transient in nature, the hydrogel becomes viscoplastic; the higher the content of temporary cross-links, the higher the stress relaxation.

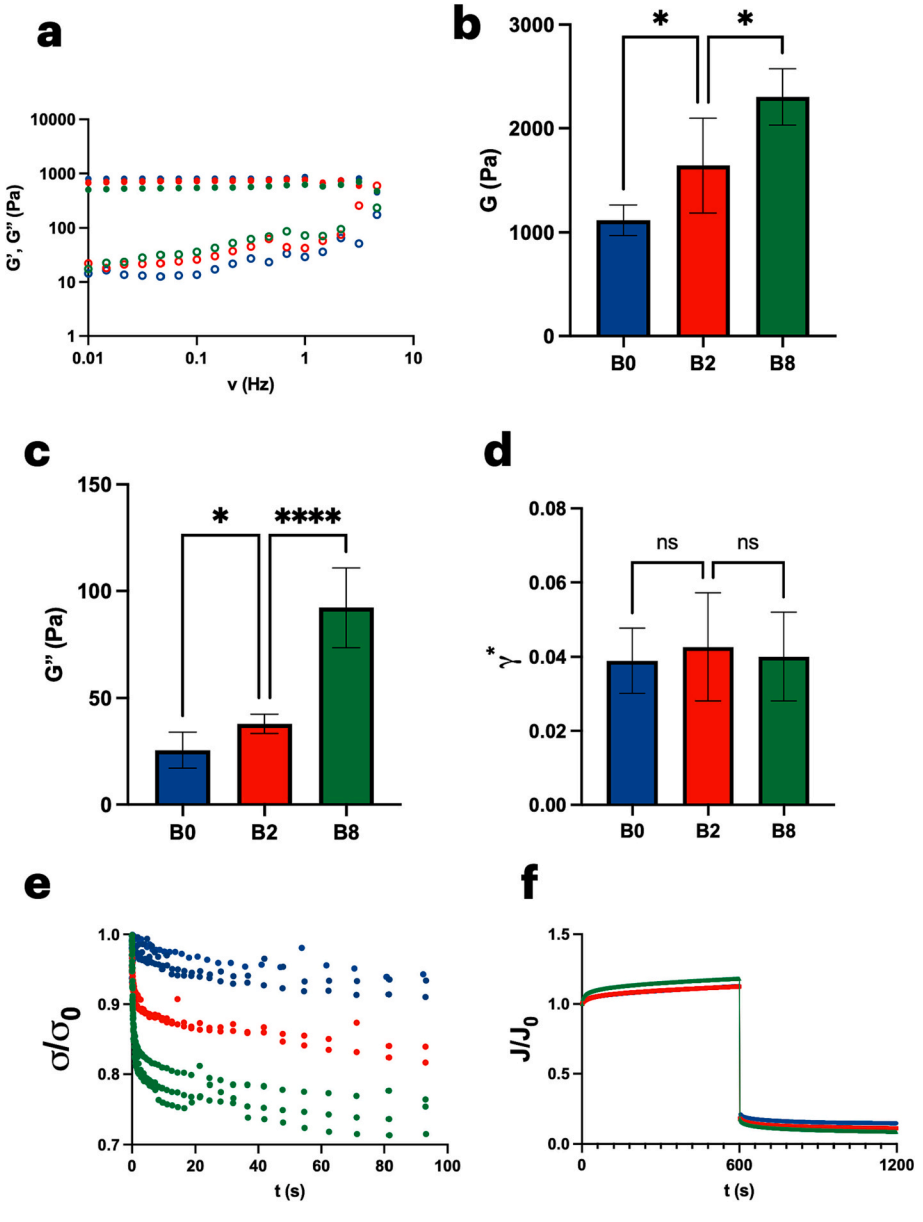

Fig. 1. Combination of permanent and temporary cross-links modulates the mechanical response of a lactose-modified chitosan (CTL) hydrogel system. (a) Sample-case of mechanical spectra with the dependence of storage (G′, filled symbols) and loss (G″, open symbols) moduli from frequency for B0, B2 and B8. (b) Shear modulus calculated by means of Eq. 3 in the main text; data are reported as mean ± s.d., n = at least 5 hydrogels analyzed for each experimental condition. (c) Loss modulus measured at 1 Hz and (d) critical strain, γ^*, obtained from long stress sweep measurements. In (c) and (d) data are reported as mean ± s.d., n = at least 10 hydrogels analyzed for each experimental condition. Statistics: Unpaired Mann-Whitney test; ns, not significant; *, $p < 0.05$; ****, $p < 0.0001$. (e) Relative variation of the stress relaxation ($\sigma/\sigma_{t=0}$) over time; for each sample, three replicates are reported. (f) Relative variation of the compliance ($J/J_{t=0}$) over time; each curve is the average of at least 5 replicates. In Supplementary material the single curves are reported with the s.d. for each time-point (Fig. S4 in Supplementary material section). Color code: B0 (black), B2 (blue) and B8 (red).

homogeneous and clear network, avoiding phase separation phenomena (Furlani, Sacco, Cok, et al., 2019). The resulting hydrogel system is transient in nature, with boric acid behaving like an (associative) weak "sticker" that binds and dissociates in a highly dynamic manner. Thus, while the introduction of the same amount of genipin in the hydrogels contributes to the elastic response of the material through the establishment of stable covalent bonds, the boric acid modulates the viscous response when stresses/deformations are applied over time (Scheme 1).

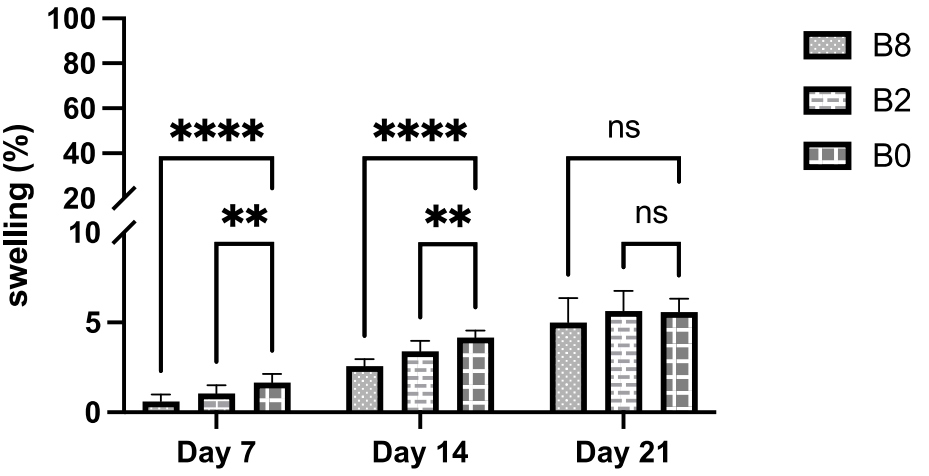

Fig. 2. Swelling over time of temporary/permanent dual cross-link hydrogels. Swelling (%) for hydrogels with different composition after 21 days of incubation in cell culture conditions. Data are reported as mean ± s.d., $n = 12$ replicates analyzed for each experimental condition. Statistics: One-Way ANOVA followed by Dunnett's multiple comparison *post hoc* test; ns, not significant; **, $p < 0.01$; ****, $p < 0.0001$.

3.2. Mechanical response of temporary/permanent dual cross-linked hydrogels

In the present work, three different hydrogels containing the same amount of genipin but different amounts of boric acid, ranging from 0 mM to 8 mM, were considered (Table S1 in the Supplementary material). For the sake of clarity, the hydrogel samples are termed hereafter as B0 (without boric acid), B2 (2 mM of boric acid) and B8 (8 mM of boric acid). Fig. 1a shows that the mechanical spectra of the three samples slightly differ. Experimental data were analyzed using the generalized Maxwell model, which consists of a sequence of Maxwell elements (spring and dashpot) connected in parallel with an additional spring, as previously reported (Turco et al., 2011). The storage and loss moduli are modelled as a function of pulsation, ω, using the following equations (Eqs. 1 and 2):

$$G' = G_e + \sum_{i=1}^{n} G_i \frac{(\lambda_i \omega)^2}{1 + (\lambda_i \omega)^2}; G_i = \frac{\eta_i}{\lambda_i} \tag{1}$$

$$G'' = \sum_{i=1}^{n} G_i \frac{\lambda_i \omega}{1 + (\lambda_i \omega)^2} \tag{2}$$

with n the number of the Maxwell elements considered, G_i, η_i, and λ_i the spring constant, the dashpot viscosity, and the relaxation time of the ith Maxwell element, respectively. G_e is the additional spring constant. Three Maxwell elements accurately modelled the experimental data for B0, B2 and B8, respectively.

This approach allows determining the shear modulus, G, as (Eq. 3):

$$G = G_e + \sum_{1=1}^{n} G_i \tag{3}$$

While the purely elastic response in terms of *Ge* and Young's modulus is the same for all three samples (Figs. S1a and S9 in the Supplementary material section), small differences are observed for the shear modulus G (Fig. 1b). The addition of boric acid leads to an increase in the elastically active segments, and hence in the shear modulus, due to the binding to diols in the side chain of the polysaccharide. However, all hydrogels considered are soft, with a shear modulus below 3 kPa. Recently, it was shown that myoblasts activity is not affected by the initial elastic modulus of the substrate when it is lower than about 12 kPa (Bauer et al., 2017). Therefore, the differences in G detected for B0, B2 and B8 hydrogels are not expected to substantially influence cell behaviour.

The relaxation times calculated from Eqs. 1 and 2 depend on the composition of the hydrogels. As an example, the introduction of boric acid progressively reduces λ_1, the shortest relaxation time, from $9.5{\cdot}10^{-3}$ s to $4.7{\cdot}10^{-3}$ s (Fig. S1b and Table S2 in Supplementary material section), due to the transient cross-links with the diols in the CTL side chain (Furlani, Sacco, Scognamiglio, et al., 2019). The effect of boric acid on the elastic components calculated from Eqs. 1 and 2 is more pronounced for the shortest relaxation time, thus determining the experimental profile of the mechanical spectrum at higher frequency values (Fig. S2a–c in the Supplementary material section). In this case, the rate of mechanical stimulation is comparable to or higher than the binding/unbinding rate of boric acid (Sacco, Furlani, et al., 2020). In contrast, the effect of the temporary cross-linker at the higher relaxation time λ_3, although still present in B8, is much less pronounced.

The contributions to the overall viscosity from the three Maxwell elements are shown in Fig. S3a–d in the Supplementary material section. The presence of boric acid increases the viscosity of the first and second Maxwell elements, corresponding to the fastest and second-fastest relaxation time. The presence of boric acid thus affects the relative molecular motions at medium to high frequency due to the rapid binding and unbinding to the diols of CTL (Sacco, Furlani, et al., 2020). The effect of boric acid is negligible for the third Maxwell element, *i.e.* the one with the longer relaxation times. In this case, the molecular motions occur on a scale of tens of seconds, which is far too slow to be affected by the transient binding of boric acid. Overall, the sum of all viscous terms shows no differences between the samples, as the main contribution in numerical terms comes from the third Maxwell element (Fig. S3d in the Supplementary material section).

Long stress sweep analyses strengthen these conclusions. Both the storage (G') and the loss modulus (G'') are measured at a frequency of 1 Hz, *i.e.* comparable to the relaxation time of the second Maxwell element, λ_2. Fig. 1c shows the trend of the loss modulus for B0, B2 and B8, respectively, which parallels the viscosity of the second Maxwell element, with the presence of boric acid increasing the viscous response. However, this trend only holds for the frequency used for the stress sweep analyses. The presence of boric acid and the temporary cross-links have no effect on the critical strain (Fig. 1d), *i.e.* the strain at which the linear stress-strain relationship is lost (Sacco, Baj, et al., 2020).

An additional comparison of the three different hydrogels was carried out using stress relaxation and creep compliance experiments (Fig. 1e and f). The stress relaxation curves indicate the presence of temporary cross-links in the structure of the hydrogels containing boric acid (Fig. 1e). The B0 hydrogel, which contains only permanent cross-links (genipin), shows limited relaxation of stress over the timeframe studied, as expected for a highly elastic structure. In contrast, the presence of boric acid at a concentration of 2 mM (B2) or 8 mM (B8)

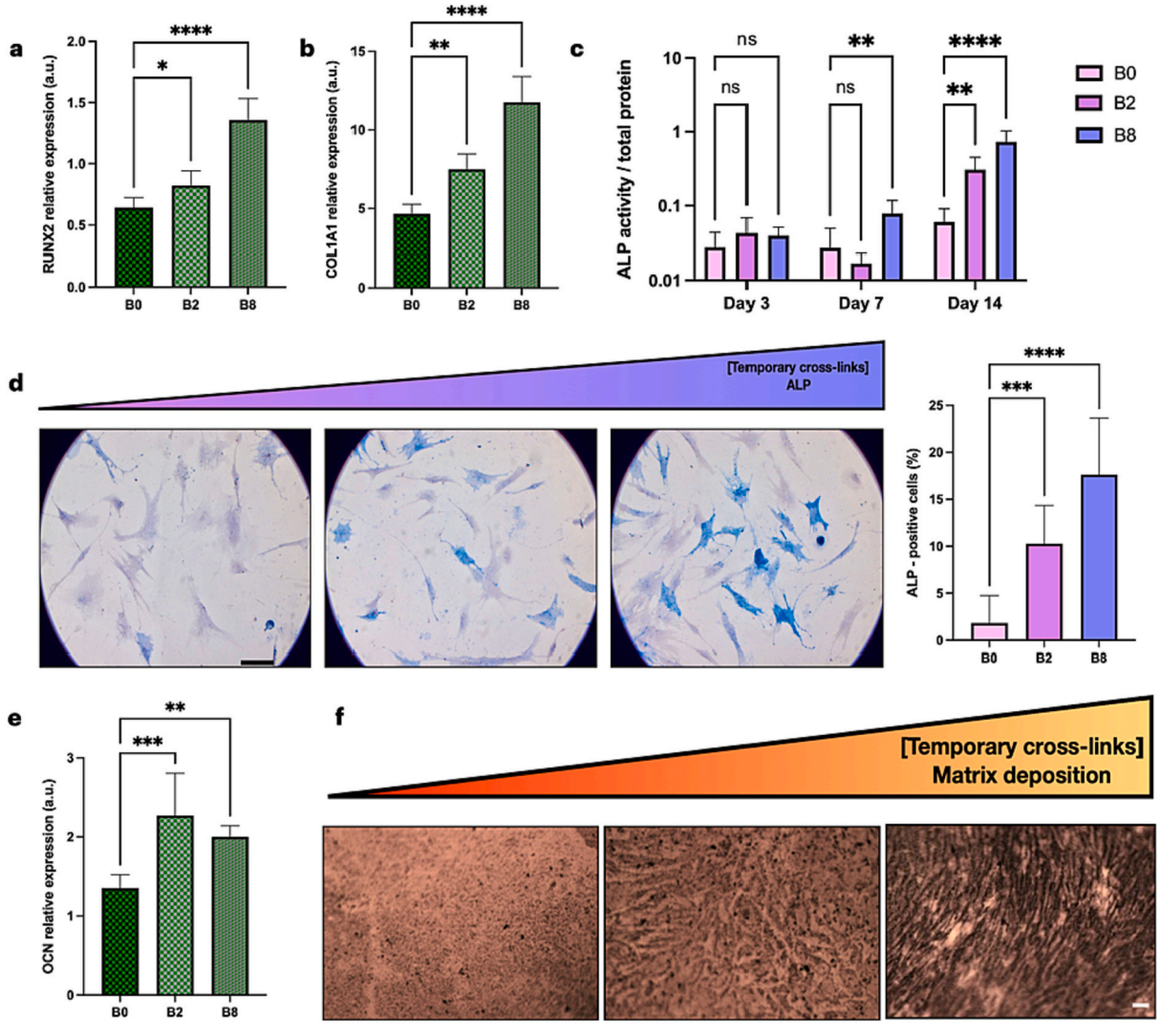

Fig. 3. Increased content of temporary cross-links fosters the osteogenic commitment of adipose-derived mesenchymal stem cells. Relative gene expression quantification (arbitrary units, a.u.) of runt-related transcription factor 2 (RUNX2) (a) and collagen 1 (COL1A1) (b) in cells grown on B0, B2 and B8, respectively, after 7 days of incubation using in osteogenic medium. Data are reported as mean ± s.d., $n = 6$–10 replicates analyzed for each experimental condition. (c) Quantification of alkaline phosphatase (ALP) enzyme activity after 3, 7 and 14 days of incubation in osteogenic medium. Data are reported as mean ± s.d., $n = 6$–12 replicates analyzed for each time point. (d) Representative images and quantification of positive cells to ALP detected by Fast blue staining, indicating the osteogenic differentiation of mesenchymal stem cells after 14 days of incubation in osteogenic medium; scale bar is 100 μm. Data are reported as mean ± s.d., $n = 17$–25 images analyzed for each experimental condition. (e) Relative gene expression quantification (arbitrary units, a.u.) of osteocalcin (OCN) after 7 days of incubation in osteogenic medium. Data are reported as mean ± s.d., $n = 6$–8 replicates analyzed for each experimental condition. (f) Representative images of calcium deposits detected by Von Kossa staining for hydrogels with different degree of plasticity after 14 days of incubation in osteogenic medium; scale bar is 50 μm. Statistics: One-Way ANOVA followed by Dunnett's multiple comparisons test; ns, not significant; *, $p < 0.05$; **, $p < 0.01$; ***, $p < 0.001$; ****, $p < 0.0001$.

causes an almost immediate relaxation of the stress; the higher the amount of boric acid, the more pronounced the immediate drop in stress. This is ascribed to the transient nature of the boric acid cross-links as the immediate application of the stress leads to an unzipping of the bound boric acid. The effect of the boric acid is also evident to some extent in the creep compliance curves (Fig. 1f). While B2 shows no differences from B0 in this case, a further increase in boric acid content, *i.e.* with B8, leads to an increase in strain after 600 s that is statistically different from the previous samples. However, it is noteworthy that during the creep recovery step, all hydrogel samples regain almost their original size, with a final permanent deformation (plasticity) in the range of 8% to 14 %. As might be expected, the dynamic nature of boric acid binding leads to a rapid unzipping of cross-links when the stress is applied, but an equally rapid re-binding when it is removed.

Next, we investigated the structural stability of B0, B2 and B8, respectively. Swelling experiments performed after 21 days of incubation in cell culture medium show negligible uptake of the medium for all hydrogels examined (swelling <10%) (Fig. 2a). Taken together, these results demonstrate a material approach suitable for the development of soft viscoplastic hydrogels with varying degrees of immediate stress relaxation without significant swelling.

3.3. Increased content of temporary cross-links guides the osteogenic commitment of stem cells

Next, we investigated the influence of the content of temporary cross-links (boric acid) in the hydrogels on the osteogenic commitment of human adipose-derived mesenchymal stem cells (hMSC-AT) cultured under 2D-conditions, with highly elastic hydrogels (*i.e.* those containing only genipin without boric acid, B0) as a control. hMSC-AT were chosen as a model due to their osteogenic potential in terms of extracellular matrix mineralization, osteocalcin expression and alkaline phosphatase

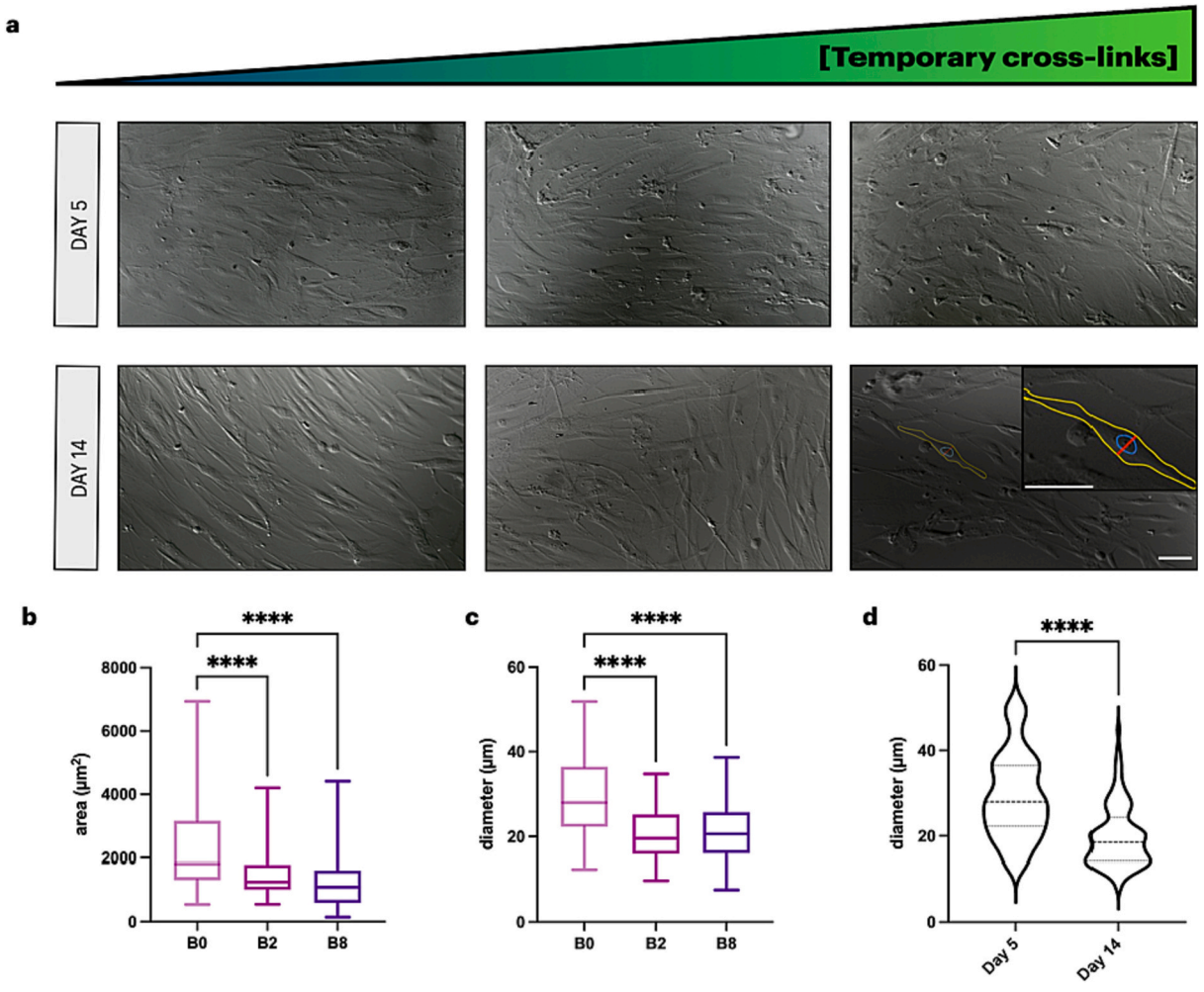

Fig. 4. Reduced content of temporary cross-links fosters the spreading of adipose-derived mesenchymal stem cells. (a) Representative images of mesenchymal stem cells plated atop B0, B2 and B8, respectively, after 5 and 14 days of incubation in osteogenic medium. Zoom-in/inset: yellow, cell area; blue: nucleus; red: cell minor axis. Scale bars are 70 μm. (b) Cell spreading area and (c) diameter of the minor axis for hydrogels with different composition after 5 days of incubation in osteogenic medium. Data are reported as mean ± s.d., $n = 73–94$ cells analyzed in (b) and $n = 60–77$ in (c). Statistics: One-way ANOVA followed by Dunnett's multiple comparison *post hoc* test; ****, $p < 0.0001$. (d) Time-comparison of minor axis diameter of cells on B0 hydrogels. Data are reported as violin plots showing the median of values, $n = 76–104$ cells analyzed for each experimental condition. Statistics: Unpaired two tailed *t*-test; ****, $p < 0.0001$.

(ALP) production (Im, Shin, & Lee, 2005). Stem cells were seeded on fibronectin-coated hydrogels with different amounts of boric acid, namely B0, B2 and B8, respectively. The cells were then treated with an osteogenic medium (Chaudhuri et al., 2016; Langenbach & Handschel, 2013).

First, the osteogenic potential of hMSC-AT was investigated by gene expression analysis. Runt-related transcription factor 2 (RUNX2), an osteogenic regulator that plays a crucial role in osteoblastic differentiation (Bruderer, Richards, Alini, & Stoddart, 2014), was selected as an early marker of bone formation. After seven days of cell culture, we observed a clear dependence of RUNX2 expression on the content of boric acid in the hydrogel (Fig. 3a), indicating that hMSC-AT are committed to differentiate with increasing boric acid content. This was confirmed by quantifying the relative expression of another early osteogenic marker such as type-1 collagen (COL1A1) (Fig. 3b) (Bruderer et al., 2014).

We also quantified the production of the enzyme ALP over a fourteen-day period (Fig. 3c). After three days, negligible differences (and basal production) were observed regardless of hydrogel type, consistent with an immature osteoprogenitor phenotype (Huang, Yang, Shao, & Li, 2007). As incubation time increases up to seven days, only B8 hydrogels begin to promote a significant increase in ALP production. This effect becomes evident after fourteen days of incubation and a clear dependence of the ALP activity on the composition of the hydrogel becomes apparent. While the cells growing on B0 show minimal ALP activity, the cells growing on B8 exhibit a 20-fold increase of enzymatic activity. Remarkably, these results were qualitatively confirmed by Fast Blue staining and the calculation of ALP-positive cells (Fig. 3d).

Next, we examined downstream events such as the expression of the late osteogenic marker osteocalcin (OCN) and the production of mineralized matrix. Again, we found that B8 elicited 3-fold higher relative expression of OCN than B0 (Fig. 3e). These observations are consistent with the production of mineralized matrix (calcium deposits) by the cells, as detected by Von Kossa staining (Fig. 3f). We also excluded that stem cells differentiated into other cell phenotypes by testing for their adipogenic or chondrogenic lineage, by using Oil Red O staining and quantifying the relative expression of SOX9 (Supplementary material, Fig. S5) and lipoprotein lipase (LPL) (values below detection limit). We also ruled out a different proliferation rate of the cells over the time period studied (Supplementary material, Fig. S6). Collectively, our results show that hydrogel composition in terms of temporary cross-links content, and thus immediate dissipation of stress, is a crucial material trait that controls the osteogenic commitment of stem cells with negligible impact on proliferation.

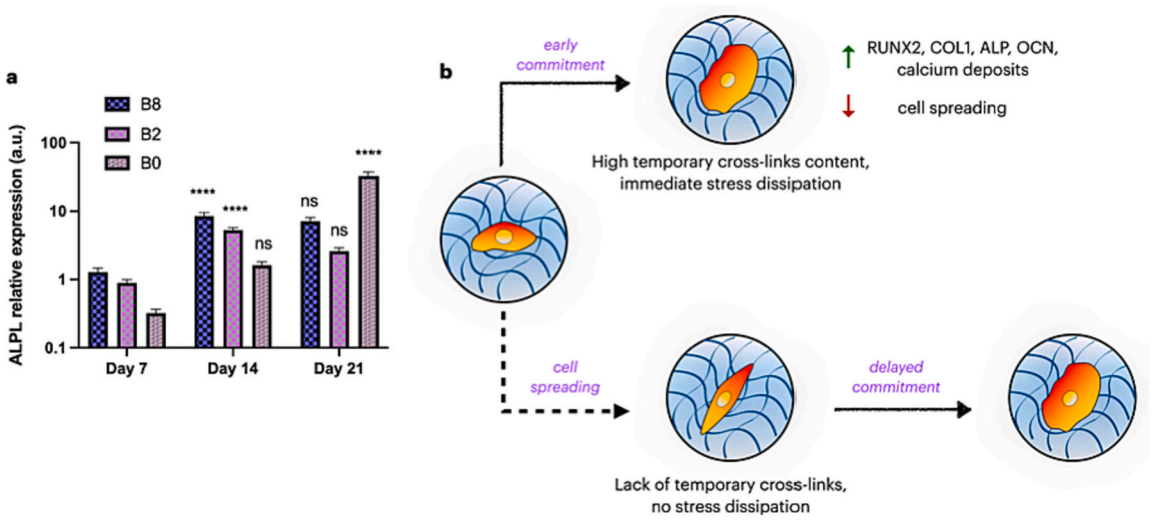

Fig. 5. Immediate stress dissipation due to temporary cross-links accelerates the osteogenic commitment of mesenchymal stem cells. (a) Relative gene expression quantification of alkaline phosphatase (ALP) in cells grown on B0, B2, and B8 hydrogels, respectively. Data are reported as mean ± s.d., $n = 6$ replicates analyzed for each experimental condition. Statistics: One-Way ANOVA followed by Tukey's multiple comparisons test; ns, not significant; ****, $p < 0.0001$. (b) Cartoon schematic recapitulating what identified in this study. After anchoring on the hydrogel, the mesenchymal stem cells decide whether to start differentiating or spreading depending on the immediate dissipation of stresses. In dissipative hydrogels containing high amounts of transient cross-links, the cells are committed to early differentiate with only moderate effects on cell morphology; this is accompanied with the upregulation of osteogenic markers and the mineralization of the matrix. In contrast, non-dissipative (elastic) hydrogels promote cell spreading, with negligible osteogenic commitment over comparable time periods. Importantly, the osteogenic commitment of mesenchymal stem cells in non-dissipative hydrogels occurs later, suggesting a chronologically dependent triggering of the osteogenic cascade.

It has been previously reported that important changes in viscosity have a crucial impact on cell biology (Cameron et al., 2011; Charrier et al., 2018; Nguyen, Sun, Yokota, & Lin, 2021). We have shown here that the sum of all viscous terms shows no differences between the samples (Fig. S3d in the Supplementary material). However, the presence of boric acid increases the viscosity at relatively fast relaxation times. It is likely that, in our case, the cells perceive this rapid mechanotransduction events thereby showing a similar viscosity sensing (Bennett et al., 2018). This is supported by the fast – on a relative scale – stress relaxation in the B8 samples (Fig. 1e), which is known to be an important regulator of cell activity (Chaudhuri et al., 2016).

The viscoplasticity of the hydrogel is also expected to influence cell fate in terms of spreading (Grolman et al., 2020). Since the latter has similarly viscous, complex processes and involves changes in the stress fibers of the cytoskeleton (Fan et al., 2021), we wondered whether cell morphology could be related to the degree of stem cell differentiation. Previous studies have indeed shown that mesenchymal stem cells become more elongated when differentiating into osteoblasts (Docheva et al., 2008; Stavenschi & Hoey, 2019). To test this, stem cells were seeded under subconfluent conditions on the three hydrogels with different amounts of transient cross-links and their morphology was examined after five days using bright field microscopy. The analysis of images revealed that both the cell spreading area and the minor axis diameter are larger on B0 (Fig. 4a–c) where osteogenic commitment is lower. Thus, it appears that hMSC-AT prefer to remodel components of the cytoskeleton in purely elastic hydrogels rather than start to differentiate in the early stages of incubation.

Strikingly, the minor axis diameter decreased only in cells plated on B0 while incubation lasted up to fourteen days (Fig. 4d and Supplementary Material, Fig. S7), suggesting a delayed differentiation of hMSC-AT. To test this evidence, we extended the incubation of hMSC-AT under osteogenic culture conditions up to twenty-one days. As expected, we found that the expression of ALP gene do not increase from day 14 to day 21 in cells seeded on B2 and B8, respectively, consistent with the typical trend of this marker during osteogenic differentiation (Huang et al., 2007). In contrast, ALP increases significantly in B0 (Fig. 5a). This result is supported by the simultaneous up-regulation of the relative expression of RUNX2 (Supplementary material, Fig. S8). From these observations, it can be concluded that the osteogenic commitment of hMSC-AT is temporally modulated by the hydrogel type: while hydrogels with immediate stress (energy) dissipation promote early commitment of mesenchymal stem cells due to the abundance of transient cross-links, highly elastic (non-dissipative) hydrogels delay the entire process (Fig. 5b).

4. Conclusions

It is well known that cells sense the mechanics of the extracellular matrix around them and respond accordingly (Brusatin et al., 2018; Discher et al., 2005, 2009; Dupont et al., 2011; Engler et al., 2006; Mammoto & Ingber, 2010; Panciera et al., 2017; Swift et al., 2013). Here, our results show a strong correlation between the immediate stress (energy) dissipation due to rapid unbinding of transient cross-links in dual cross-link hydrogels and the osteogenic commitment of adipose-derived mesenchymal stem cells cultured in 2D conditions. We used a hydrogel system with a mixture of permanent/temporary cross-links, whose viscoplasticity is adjustable by the dynamics of binding/unbinding of the temporary cross-linker. By varying the amount of boric acid, we have produced hydrogels ranging from essentially purely elastic to dissipative and viscoelastic. By using these materials as 2D-hydrogel substrates for cell culture, we have shown that the presence of transient cross-links of the hydrogel can temporally regulate the osteogenic commitment of mesenchymal stem cells. Cell growth on hydrogel with immediate stress (energy) dissipation, *i.e.* higher transient cross-linker content, is associated with early expression of osteogenic markers and matrix mineralization. In contrast, the osteogenic commitment is delayed in cells grown on purely elastic hydrogels. In this case, cells spread out more widely before starting to differentiate. Overall, our results show that, in addition to stiffness and viscoelasticity (Chaudhuri et al., 2016; Steward & Kelly, 2015), the presence of transient cross-links and the consequent immediate stress dissipation upon application of stress has a significant impact on the osteogenic commitment of mesenchymal stem cells and represents an optimal starting point for future mechanotransduction studies.

CRediT authorship contribution statement

C.P. performed mechanical and biological experiments, analyzed the results and wrote the original draft of the paper; F.S. performed part of cell culture studies and helped with the discussion of results; P.S. designed the study, analyzed and interpreted the results, wrote the final draft of the paper; S.L. performed part of mechanical investigation and carried out preliminary differentiation experiments; M.R. performed quantitative Real Time PCR (qPCR), analyzed and interpreted the results; I.D. supervised mechanical experiments and helped with the interpretation of results; E.M. designed biological experiments, supervised biological experiments and helped with the interpretation of results.

Declaration of competing interest

The authors declare that they have no known competing financial interests or personal relationships that could have appeared to influence the work reported in this paper.

Data availability

Data will be made available on request.

Acknowledgments

The financial support to F.S. (Fellowship: "Materiali meccano-trasduttivi: studio degli effetti sul differenziamento di cellule mesenchimali") by the Department of Medical, Surgical and Health Sciences, University of Trieste. The financial support to P.S. (Fellowship, project: "Preparazione mediante metodi eco-sostenibili di matrici di idrocolloidi per analisi batteriologiche e virologiche" - Bando A2/2020) by AREA Science Park is gratefully acknowledged.

Appendix A. Supplementary data

Supplementary data to this article can be found online at https://doi.org/10.1016/j.carbpol.2022.120369.

References

Bauer, A., Gu, L., Kwee, B., Li, W. A., Dellacherie, M., Celiz, A. D., & Mooney, D. J. (2017). Hydrogel substrate stress-relaxation regulates the spreading and proliferation of mouse myoblasts. *Acta Biomaterialia, 62*, 82–90. https://doi.org/10.1016/J.ACTBIO.2017.08.041

Bennett, M., Cantini, M., Reboud, J., Cooper, J. M., Roca-Cusachs, P., & Salmeron-Sanchez, M. (2018). In *, 115(6). Molecular clutch drives cell response to surface viscosity* (pp. 1192–1197). https://doi.org/10.1073/pnas.1710653115

Bruderer, M., Richards, R. G., Alini, M., & Stoddart, M. J. (2014). Role and regulation of runx2 in osteogenesis. *European Cells and Materials, 28*, 269–286. https://doi.org/10.22203/eCM.v028a19

Brusatin, G., Panciera, T., Gandin, A., Citron, A., & Piccolo, S. (2018). Biomaterials and engineered microenvironments to control YAP/TAZ-dependent cell behaviour. *Nature Materials, 17*(12), 1063–1075. https://doi.org/10.1038/s41563-018-0180-8

Cameron, A. R., Frith, J. E., & Cooper-White, J. J. (2011). The influence of substrate creep on mesenchymal stem cell behaviour and phenotype. *Biomaterials, 32*(26), 5979–5993. https://doi.org/10.1016/j.biomaterials.2011.04.003

Cameron, A. R., Frith, J. E., Gomez, G. A., Yap, A. S., & Cooper-White, J. J. (2014). The effect of time-dependent deformation of viscoelastic hydrogels on myogenic induction and Rac1 activity in mesenchymal stem cells. *Biomaterials, 35*(6), 1857–1868. https://doi.org/10.1016/J.BIOMATERIALS.2013.11.023

Cantini, M., Donnelly, H., Dalby, M. J., & Salmeron-Sanchez, M. (2020). The plot thickens: The emerging role of matrix viscosity in cell mechanotransduction. *Advanced Healthcare Materials, 9*(8), 1901259. https://doi.org/10.1002/adhm.201901259

Charrier, E. E., Pogoda, K., Wells, R. G., & Janmey, P. A. (2018). Control of cell morphology and differentiation by substrates with independently tunable elasticity and viscous dissipation. *Nature Communications, 9*(1), 449. https://doi.org/10.1038/s41467-018-02906-9

Chaudhuri, O., Cooper-White, J., Janmey, P. A., Mooney, D. J., & Shenoy, V. B. (2020). Effects of extracellular matrix viscoelasticity on cellular behaviour. *Nature, 584*(7822), 535–546. https://doi.org/10.1038/s41586-020-2612-2

Chaudhuri, O., Gu, L., Darnell, M., Klumpers, D., Bencherif, S. A., Weaver, J. C., Huebsch, N., & Mooney, D. J. (2015). Substrate stress relaxation regulates cell spreading. *Nature Communications, 6*(1), 6365. https://doi.org/10.1038/ncomms7365

Chaudhuri, O., Gu, L., Klumpers, D., Darnell, M., Bencherif, S. A., Weaver, J. C., Huebsch, N., Lee, H., Lippens, E., Duda, G. N., & Mooney, D. J. (2016). Hydrogels with tunable stress relaxation regulate stem cell fate and activity. *Nature Materials, 15*(3), 326–334. https://doi.org/10.1038/nmat4489

Discher, D. E., Janmey, P., & Wang, Y.-L. (2005). Tissue cells feel and respond to the stiffness of their substrate. *Science, 310*(5751), 1139–1143. https://doi.org/10.1126/science.1116995

Discher, D. E., Mooney, D. J., & Zandstra, P. W. (2009). Growth factors, matrices, and forces combine and control stem cells. *Science, 324*(5935), 1673–1677. https://doi.org/10.1126/science.1171643

Docheva, D., Padula, D., Popov, C., Mutschler, W., Clausen-Schaumann, H., & Schieker, M. (2008). Researching into the cellular shape, volume and elasticity of mesenchymal stem cells, osteoblasts and osteosarcoma cells by atomic force microscopy: Stem cells. *Journal of Cellular and Molecular Medicine, 12*(2), 537–552. https://doi.org/10.1111/j.1582-4934.2007.00138.x

Dupont, S., Morsut, L., Aragona, M., Enzo, E., Giulitti, S., Cordenonsi, M., Zanconato, F., Le Digabel, J., Forcato, M., Bicciato, S., Elvassore, N., & Piccolo, S. (2011). Role of YAP/TAZ in mechanotransduction. *Nature, 474*(7350), 179–183. https://doi.org/10.1038/nature10137

Engler, A. J., Sen, S., Sweeney, H. L., & Discher, D. E. (2006). Matrix elasticity directs stem cell lineage specification. *Cell, 126*(4), 677–689. https://doi.org/10.1016/j.cell.2006.06.044

Fan, T., Qu, R., Jiang, X., Yang, Y., Sun, B., Huang, X., Zhou, Z., Ouyang, J., Zhong, S., & Dai, J. (2021). Spatial organization and crosstalk of vimentin and actin stress fibers regulate the osteogenic differentiation of human adipose-derived stem cells. *FASEB Journal, 35*(2), 1–16. https://doi.org/10.1096/fj.202000378RR

Furlani, F., Sacco, P., Cok, M., de Marzo, G., Marsich, E., Paoletti, S., & Donati, I. (2019). Biomimetic, multiresponsive, and self-healing lactose-modified chitosan (CTL)-based gels formed via competitor-assisted mechanism. *ACS Biomaterials Science & Engineering, 5*(10), 5539–5547. https://doi.org/10.1021/acsbiomaterials.9b01256

Furlani, F., Sacco, P., Scognamiglio, F., Asaro, F., Travan, A., Borgogna, M., Marsich, E., Cok, M., Paoletti, S., & Donati, I. (2019). Nucleation, reorganization and disassembly of an active network from lactose-modified chitosan mimicking biological matrices. *Carbohydrate Polymers, 208*, 451–456. https://doi.org/10.1016/j.carbpol.2018.12.096

Grolman, J. M., Weinand, P., & Mooney, D. J. (2020). Extracellular matrix plasticity as a driver of cell spreading. *Proceedings of the National Academy of Sciences of the United States of America, 117*(42), 25999–26007. https://doi.org/10.1073/pnas.2008801117

Huang, W., Yang, S., Shao, J., & Li, Y. P. (2007). Signaling and transcriptional regulation in osteoblast commitment and differentiation. *Frontiers in Bioscience, 12*(8), 3068–3092. https://doi.org/10.2741/2296

Im, G. I., Shin, Y. W., & Lee, K. B. (2005). Do adipose tissue-derived mesenchymal stem cells have the same osteogenic and chondrogenic potential as bone marrow-derived cells? *Osteoarthritis and Cartilage, 13*(10), 845–853. https://doi.org/10.1016/j.joca.2005.05.005

Jia, Y., Wang, Y., Niu, L., Zhang, H., Tian, J., Gao, D., Zhang, X., Lu, T. J., Qian, J., Huang, G., & Xu, F. (2021). The plasticity of nanofibrous matrix regulates fibroblast activation in fibrosis. *Advanced Healthcare Materials, 10*(8). https://doi.org/10.1002/ADHM.202001856

Langenbach, F., & Handschel, J. (2013). Effects of dexamethasone, ascorbic acid and β-glycerophosphate on the osteogenic differentiation of stem cells in vitro. *Stem Cell Research & Therapy, 4*(5), 117. https://doi.org/10.1186/scrt328

Lee, H., Gu, L., Mooney, D. J., Levenston, M. E., & Chaudhuri, O. (2017). Mechanical confinement regulates cartilage matrix formation by chondrocytes. *Nature Materials, 16*(12), 1243–1251. https://doi.org/10.1038/nmat4993

Mammoto, T., & Ingber, D. E. (2010). Mechanical control of tissue and organ development. *Development, 137*(9), 1407–1420. https://doi.org/10.1242/dev.024166

Marozas, I. A., Anseth, K. S., & Cooper-White, J. J. (2019). Adaptable boronate ester hydrogels with tunable viscoelastic spectra to probe timescale dependent mechanotransduction. *Biomaterials, 223*, Article 119430. https://doi.org/10.1016/j.biomaterials.2019.119430

Marozas, I. A., Cooper-White, J. J., & Anseth, K. S. (2019). Photo-induced viscoelasticity in cytocompatible hydrogel substrates. *New Journal of Physics, 21*(4), Article 045004. https://doi.org/10.1088/1367-2630/ab1309

Mohammadi, H., Arora, P. D., Simmons, C. A., Janmey, P. A., & McCulloch, C. A. (2015). Inelastic behaviour of collagen networks in cell–matrix interactions and mechanosensation. *Journal of the Royal Society Interface, 12*(102). https://doi.org/10.1098/RSIF.2014.1074

Nam, S., Lee, J., Brownfield, D. G., & Chaudhuri, O. (2016). Viscoplasticity enables mechanical remodeling of matrix by cells. *Biophysical Journal, 111*(10), 2296–2308. https://doi.org/10.1016/j.bpj.2016.10.002

Nguyen, H. D., Sun, X., Yokota, H., & Lin, C. C. (2021). Probing osteocyte functions in gelatin hydrogels with tunable viscoelasticity. *Biomacromolecules, 22*(3), 1115–1126. https://doi.org/10.1021/acs.biomac.0c01476

Notbohm, J., Lesman, A., Tirrell, D. A., & Ravichandran, G. (2015). Quantifying cell-induced matrix deformation in three dimensions based on imaging matrix fibers. *Integrative Biology, 7*(10), 1186–1195. https://doi.org/10.1039/C5IB00013K

Panciera, T., Azzolin, L., Cordenonsi, M., & Piccolo, S. (2017). Mechanobiology of YAP and TAZ in physiology and disease. *Nature Reviews Molecular Cell Biology, 18*(12), 758–770. https://doi.org/10.1038/nrm.2017.87

Petroll, W. M., Cavanagh, H. D., & Jester, J. V. (2004). Dynamic three-dimensional visualization of collagen matrix remodeling and cytoskeletal organization in living corneal fibroblasts. *Scanning, 26*(1), 1–10. https://doi.org/10.1002/SCA.4950260102

Pizzolitto, C., Cok, M., Asaro, F., Scognamiglio, F., Marsich, E., Lopez, F., Donati, I., & Sacco, P. (2020). On the mechanism of genipin binding to primary amines in lactose-modified chitosan at neutral pH. *International Journal of Molecular Sciences, 21*(18), 6831. https://doi.org/10.3390/ijms21186831

Porrelli, D., Gruppuso, M., Vecchies, F., Marsich, E., & Turco, G. (2021). Alginate bone scaffolds coated with a bioactive lactose modified chitosan for human dental pulp stem cells proliferation and differentiation. *Carbohydrate Polymers, 273*(March), Article 118610. https://doi.org/10.1016/j.carbpol.2021.118610

Sacco, P., Baj, G., Asaro, F., Marsich, E., & Donati, I. (2020). Substrate dissipation energy regulates cell adhesion and spreading. *Advanced Functional Materials*. , Article 2001977. https://doi.org/10.1002/adfm.202001977

Sacco, P., Cok, M., Scognamiglio, F., Pizzolitto, C., Vecchies, F., Marfoglia, A., Marsich, E., & Donati, I. (2020). Glycosylated-chitosan derivatives: A systematic review. *Molecules, 25*(7), 1534. https://doi.org/10.3390/MOLECULES25071534

Sacco, P., Furlani, F., Marfoglia, A., Cok, M., Pizzolitto, C., Marsich, E., & Donati, I. (2020). Temporary/permanent dual cross-link gels formed of a bioactive lactose-modified chitosan. *Macromolecular Bioscience*. , Article 2000236. https://doi.org/10.1002/mabi.202000236

Sacco, P., Furlani, F., Paoletti, S., & Donati, I. (2019). pH-assisted gelation of lactose-modified chitosan. *Biomacromolecules, 20*(8), 3070–3075. https://doi.org/10.1021/acs.biomac.9b00636

Stavenschi, E., & Hoey, D. A. (2019). Pressure-induced mesenchymal stem cell osteogenesis is dependent on intermediate filament remodeling. *FASEB Journal, 33*(3), 4178–4187. https://doi.org/10.1096/fj.201801474RR

Steward, A. J., & Kelly, D. J. (2015). Mechanical regulation of mesenchymal stem cell differentiation. *Journal of Anatomy, 227*(6), 717–731. https://doi.org/10.1111/JOA.12243

Swift, J., Ivanovska, I. L., Buxboim, A., Harada, T., Dingal, P. C. D. P., Pinter, J., Pajerowski, J. D., Spinler, K. R., Shin, J.-W., Tewari, M., Rehfeldt, F., Speicher, D. W., & Discher, D. E. (2013). Nuclear lamin-A scales with tissue stiffness and enhances matrix-directed differentiation. *Science, 341*(6149). https://doi.org/10.1126/science.1240104, 1240104-1240104.

Turco, G., Donati, I., Grassi, M., Marchioli, G., Lapasin, R., & Paoletti, S. (2011). Mechanical spectroscopy and relaxometry on alginate hydrogels: A comparative analysis for structural characterization and network mesh size determination. *Biomacromolecules, 12*(4), 1272–1282. https://doi.org/10.1021/bm101556m

Wisdom, K. M., Adebowale, K., Chang, J., Lee, J. Y., Nam, S., Desai, R., Rossen, N. S., Rafat, M., West, R. B., Hodgson, L., & Chaudhuri, O. (2018). Matrix mechanical plasticity regulates cancer cell migration through confining microenvironments. *Nature Communications, 9*(1), 4144. https://doi.org/10.1038/s41467-018-06641-z